Helical spin structure of $Mn_{1-y}Fe_ySi$ under a magnetic field: Small angle neutron diffraction study

S. V. Grigoriev,[1] V. A. Dyadkin,[1] E. V. Moskvin,[1,2] D. Lamago,[3,4] Th. Wolf,[4] H. Eckerlebe,[5] and S. V. Maleyev[1]
[1]*Petersburg Nuclear Physics Institute, Gatchina, 188300 St. Petersburg, Russia*
[2]*Helmholtz-Zentrum Berlin, 14109 Berlin, Germany*
[3]*Laborotorie Léon Brellouin, 91191 Saclay, France*
[4]*Institut für Festkörperphysik, Forschungszentrum Karlsruhe, D-76021 Karlsruhe, Germany*
[5]*GKSS Forschungszentrum, 21502 Geesthacht, Germany*
(Received 19 January 2009; published 15 April 2009)

The magnetic structure of the noncentrosymmetric cubic magnets with Dzyaloshinskii-Moriya interaction $Mn_{1-y}Fe_ySi$ with $y=0.0, 0.06, 0.08, 0.10$ has been studied by means of the small angle neutron diffraction and magnetization measurements. The compounds order in the spin helix structure below T_c that decreases linearly with the Fe doping and approaches zero at $y>0.13$. We build the $(H\text{-}T)$ phase diagrams for each compound and interpret them on the basis of the Bak-Jensen hierarchical model of the principal interactions. Among these interactions are the spin-wave stiffness that decreases linearly with y, obviously duplicating the change of T_c, and the Dzyaloshinskii interaction showing the moderate evolution with y. It is shown that these compounds undergo the transition from the paramagnetic to helimagnetic phase through the intermediate chiral fluctuating phase. The discussion is given on the comparison of the $(T\text{-}P)$ phase diagram in pure MnSi and $(T\text{-}y)$ phase diagram of the $Mn_{1-y}Fe_ySi$ compounds showing the role of the principal interactions on the critical temperature T_c of these systems.

DOI: 10.1103/PhysRevB.79.144417 PACS number(s): 75.25.+z, 61.05.fg, 75.30.Kz, 75.40.−s

I. INTRODUCTION

The magnetic and transport properties of MnSi, the noncentrosymmetric cubic magnet with the space group $P2_13$, have been a subject of intensive investigations for several decades. The first wave of the interest was devoted to the origin of the magnetic structure ordering below $T_c=29$ K in a left-handed spiral along the $\langle 111\rangle$ directions with a propagation vector $k=0.36$ nm^{-1} at $T=4$ K.[1–3] The spin helicity had been understood to be a result of the equilibrium between the isotropic ferromagnetic exchange interaction and the antisymmetric Dzyaloshinski-Moriya (DM) interaction caused by the lack of a symmetry center in Mn atomic arrangement.[4–7] These two interactions are considered isotropic themselves but another weak anisotropic exchange (AE) interaction pins a direction of the helix along one of the cube diagonals.[5] This hierarchical model of interactions had explained most, if not all, experimental facts known at that time. The calmed down interest had been triggered again by the discovery of the quantum phase transition (QPT) under applied pressure and non-Fermi-liquid behavior of charge carriers at the QPT.[8–10] The second wave of interest heated up by the possible application of MnSi and relative systems[11,12] in modern spintronic devices, seems, reaches its maximum today although neither the role of the DM interaction in this QPT was clarified nor any other parameter, which would be responsible for it, has been established up to now. Since neither ferromagnetic exchange interaction nor DM interaction change under applied pressure the QPT must be governed by the unknown "hidden" parameter.

A possible candidate for this parameter has been recently suggested in Ref. 13, where the small spin-wave gap was introduced. The author of Ref. 13 has shown that the helix structure is intrinsically unstable with respect to the small magnetic field applied perpendicular to the helix wave vector **k** unless it is stabilized via a small gap in the spin-wave spectrum. Luckily for these systems, the spin-wave interaction in presence of the DM interaction guarantees appearance of a small but positive gap of order of D^2/A, where D is the strength of DM interaction and A is the spin-wave stiffness at large momenta. However, the magnetoelastic interaction gives always a negative contribution to the gap.[14] These different contributions to the gap compete and the gap may get closed at certain conditions, for example, under increasing pressure, thus destabilizing the system and driving it to the QPT.

In accord to the well established hierarchical model,[5] the cubic magnets without center of symmetry find their equilibrium in the helical ordering with the helix wave vector

$$k = SD/A. \tag{1}$$

The microscopic theory for these systems under magnetic field was recently developed,[13] where the ground-state energy and the spin-wave spectrum were evaluated. It is remarkable that the theory is able to relate the anisotropy constant F and the spin-wave stiffness A to the critical fields H_{C1}, which suppresses the cubic anisotropy, and H_{C2}, determining the transition to the ferromagnetic state, respectively, through the following expressions:

$$g\mu_B H_{C1} \sim \frac{Fk^2}{2}, \tag{2}$$

$$g\mu_B H_{C2} = Ak^2 \tag{3}$$

(where g is the Landè factor and μ_B is the Bohr magneton). Combining these expressions with the definition of k [Eq. (1)] one is able from the parameters of the magnetic structure

measured in the experiment (k, H_{C1}, and H_{C2}), to estimate the principal interactions of these systems, such as the spin-wave stiffness $A=g\mu_B H_{C2}/k^2$, the anisotropy constant $F \sim 2g\mu_B H_{C1}/k^2$, and the Dzyaloshinskii constant $SD=Ak$ (where S is the average spin of unit cell).

One of the most intriguing features of the (H-T) phase diagram of these compounds is the A phase. It is experimentally observed as the phenomenon of the 90° flop of the helix wave vector **k** from the direction parallel to the field axis to the direction perpendicular to it in a small pocket of the H-T phase diagram near T_c in the narrow range of the fields $H \sim H_{\mathrm{fl}}$.[15] We have related this phenomenon to the spin-wave gap caused by the DM interaction and predicted in[13]

$$\Delta \sim g\mu_B H_{\mathrm{fl}}/\sqrt{2}. \tag{4}$$

From one hand, the existence of the gap provides an explanation for the appearance of A phase in the (H-T) phase diagram of MnSi and the relative compounds. Equally, the existence of the A phase can be considered as an indirect proof for importance of the spin-wave gap predicted in the theory.

The theory given above was first applied to MnSi. As was shown in Refs. 15 and 16 the whole set of the experimental data concerning the (H-T) phase diagram can be well interpreted on the basis of this theory. Furthermore, it was able to describe the principal interactions in the relative system $Fe_{1-x}Co_xSi$ (Refs. 17 and 18) as well, where it was demonstrated that (i) the spin-wave stiffness A increases monotonously with the concentration x and demonstrate no correlation to the critical temperature T_c. The latter shows a slightly asymmetric bell-like shape as function of the Co concentration x with a maximum at $x \sim 0.35$. In its turn, the x dependence of the DM interaction, coupled to the average value of the spin, SD resembles the behavior of T_c. As will be shown below, Dzyaloshinskii constant D remains unchanged with concentration x, but S follows closely the $T_c(x)$ behavior.

The present paper is aimed to follow the change in the principal interactions in MnSi doped by Fe and afterward to determine their roles in the linear upon doping decrease in the ordering temperature. The doped compounds $Mn_{1-y}Fe_ySi$ and their magnetic properties had been studied by the Mössbauer method[19] showing that ferromagnetism disappears at $y \approx 0.15$. Two mechanisms are suggested to explain the effect of doping on the magnetic structure. In the mechanism of the localized picture Fe doping makes neighboring Mn atoms lose their spin ordering due to frustration of the exchange interaction. The disappearance of the magnetic order can be attributed to the increase in the number of nonmagnetic Mn. The itinerant picture of magnetism suggests that the replacement of Fe for Mn atoms produces an excess in a number of d electrons and magnetic moment disappears around $\Delta n_d = 0.15$. Authors of Ref. 19 are in favor of the second, itinerant, mechanism but, in our view, the first one is credible as well. From the simple symmetric consideration is known that each magnetic atom in $P2_13$ structure has six close neighbor magnetic atoms. The concentration of $y=0.15$ signifies that each sixth Mn atom is replaced by Fe and consequently all the magnetic atoms Mn of the compound possess a frustration of the exchange integral that is averaged out leading the system to a disordered state, or, the spin glass state at low temperature. In analogy to the QPT in MnSi driven by pressure at zero temperature one can consider the QPT in $Mn_{1-y}Fe_ySi$ driven by concentration at $T=0$. The transformation of the magnetic structure $Mn_{1-y}Fe_ySi$ with doping mimics rather well the changes undergoing in pure MnSi under applied pressure. Using small angle neutron scattering (SANS), Quantum Design PPMS measurements we build the (H-T) phase diagrams for the series of $Mn_{1-y}Fe_ySi$ and evaluate the effect of Fe doping on the principal interactions (such as A, D, F, and Δ). We show that the system $Mn_{1-y}Fe_ySi$ is governed by the same set of the principal interactions but in a different way as compared to its relative $Fe_{1-x}Co_xSi$ compound.

To conclude Sec. I, we remind the reader of a puzzle of the left-handed chirality of the spin helix.[1–3] One can predict that a new wave of interest will arise to these systems with DM interaction for their property of broken degeneracy of mirroring.[20]

The outline of this paper is as follows. The polarized SANS measurements are presented in Sec. II. Section III presents the (H-T) phase diagrams of the system under study and gives the concentration dependence of the principal interactions of the system. Section V presents the concluding remarks.

II. MEASUREMENTS

A. Experimental

The single crystals $Mn_{1-y}Fe_ySi$ with the concentrations $y=0.00$, 0.06, 0.08, and 0.10 were chosen for the study. These samples were the disks with a thickness of 3 mm and a diameter of 30 mm. The samples homogeneity and the single crystal mosaic were controlled by the x-ray Laue diffraction at Helmholtz-Zentrum Berlin. The crystal structure of the doped compounds $Mn_{1-y}Fe_ySi$ is the same for the crystals under study. The magnetization was measured with the Quantum Design physical properties measurement system (PPMS).

The polarized SANS experiments were carried out at the SANS-2 scattering facility of the FRG-1 research reactor in Geesthacht (Germany). A polarized beam of neutrons with an initial polarization of $P_0=0.93$, the neutron wavelength $\lambda = 0.58$ nm ($\Delta\lambda/\lambda=0.1$), and a divergence of 2.5 mrad was used. The scattered neutrons were detected by a position sensitive detector with 256×256 pixels. The detector-sample distance was set such that the Q range was covered from 6×10^{-2} to 1 nm^{-1} with a step of 0.01 nm^{-1}. We applied the magnetic field oriented perpendicularly to the incident beam, which was ranged from 0 to 800 mT.[21] The scattering intensities $[I(Q,P_0)]$ and $[I(Q,-P_0)]$ were detected with the polarization $+P_0=(+\mathbf{P}_0\mathbf{h})$ along and $-P_0=(-\mathbf{P}_0\mathbf{h})$ opposite to the magnetic field **h**. The observed Bragg reflections are characterized by two quantities: (i) the intensity

$$I(\mathbf{Q}) = [I(\mathbf{Q},P_0) + I(\mathbf{Q},-P_0)]$$

and (ii) the polarization

$$P_s(\mathbf{Q}) = \frac{[I(\mathbf{Q},P_0) - I(\mathbf{Q},-P_0)]}{[I(\mathbf{Q},P_0) + I(\mathbf{Q},-P_0)]}.$$

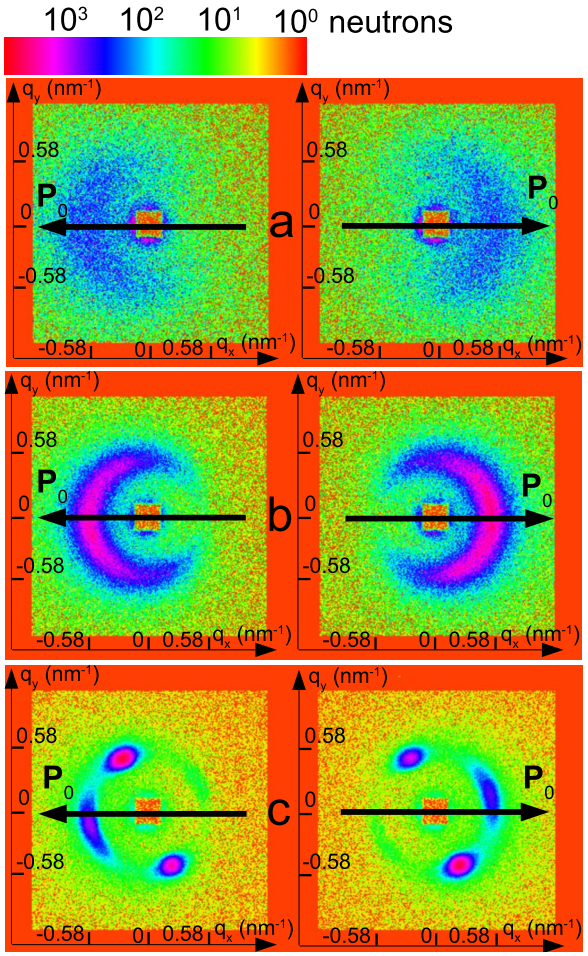

FIG. 1. (Color online) Maps of the polarized SANS intensities of the sample $Mn_{0.92}Fe_{0.08}Si$ ($T_c = 10.55 \pm 0.05$ K) for the polarization $\mathbf{P}_0$ along the guide field (left) and opposite to it (right) at $T = 14$ K (a), $T = 10.75$ K (b), $T = 8.75$ K (c).

Two types of measurements were performed in the experiment: (i) study of the temperature evolution of the helixes close to T_c in zero field and (ii) study of the effect of the magnetic field on the helix structure below T_c. Both temperature and magnetic-field evolutions are very similar for the samples under study with the only difference in the value of the critical temperature and in the magnitude of the critical fields H_{C1} and H_{C2}. Below we show the maps of SANS intensities taken from the representative compound $Mn_{0.92}Fe_{0.08}Si$ with $T_c = 10.55 \pm 0.05$ K.

B. Temperature evolution

Examples of the critical scattering for neutron polarization $\mathbf{P}_0$ along and opposite the guide field of order of 1 mT are shown in Fig. 1. The diffuse scattering at $T = 14$ K, i.e., well above T_c [Fig. 1(a)], looks like blurred spots on the left and right sides of the maps for two different polarizations $\pm\mathbf{P}_0$. The spots are transformed into the half-moon images close to T_c at $T = 10.75$ K [Fig. 1(b)]. The sum of the intensities of two opposite polarizations forms an anisotropic ring with weak spots, which below T_c transforms into the Bragg

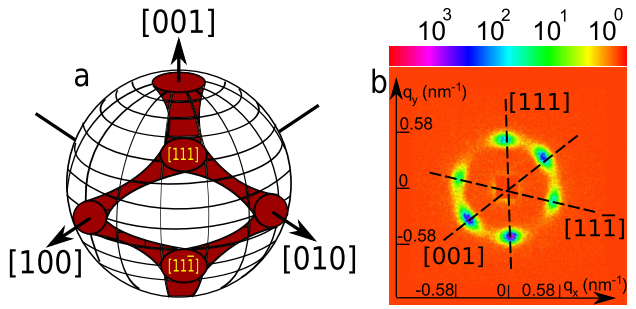

FIG. 2. (Color online) The schematic distribution of the scattered intensity on the sphere of radius $|\mathbf{k}|$ in the reciprocal space for the sample $Mn_{0.92}Fe_{0.08}Si$ (a). The SANS map taken for nonpolarized neutrons represents the cross section of the sphere by the plane $(1\bar{1}0)$ (b).

peaks, while the ring disappears [Fig. 1(c)]. It is important to not that the asymmetric P-dependent scattering is a fingerprint of the single chirality of the spin helix that corresponds to the sign of the DM interaction. The radius of the ring of intensity observed above T_c gives the value of the helix wave vector $|\mathbf{k}|$ and its width gives the inverse correlation length κ in the direction along $\mathbf{k}$. We argue that the nature of the critical fluctuations is determined by competition of two length scales: κ and the helix wave vector k. Indeed, when the full 2π twist of the helix is well established within the fluctuations ($\kappa/k < 1$), the DMI plays an important role. Hence the noncollinearity of the spin fluctuations is important close to the transition at large distances and reveals itself through the well resolved half moons in Fig. 1(b). Otherwise, the full 2π twist of the helix is not completed inside the critical fluctuation ($\kappa/k > 1$) and the fluctuations are of the ferromagneticlike nature. In this case noncollinearity is inessential and the nature of the fluctuations has to be close to that in conventional ferromagnets. This leads to smearing of half moons [Fig. 1(a)].

A typical example of the magnetic scattering at $T = 8$ K (that is below T_c) shows presence of several reflections with the differently oriented helix wave vector $\mathbf{k}$ of the same length. The couples of peaks, symmetrically disposed with respect to the origin (000), characterize domains oriented in certain direction of a crystal structure. For example, the helix wave vector of pure MnSi is clearly oriented along the $\langle 111 \rangle$ axes with the magnetic mosaic of order of 2–3 degrees.[16] The $\mathbf{k}$ vector of the doped samples has an ill-defined direction since the Bragg peaks are smeared around either $\langle 111 \rangle$ or $\langle 100 \rangle$ axes. The location of the helix wave vector $\mathbf{k}$ in the reciprocal space for the sample $Mn_{0.92}Fe_{0.08}Si$ was measured at $T = 8$ K by making the wide-range ω scan around the [111] axis. The schematic distribution of the scattered intensity on the sphere of radius $|\mathbf{k}|$ in the reciprocal space is shown in Fig. 2(a). The maxima of the intensity are observed around $\langle 111 \rangle$ and $\langle 100 \rangle$ axes. The mosaic of these maxima extends up to 10–15 degrees. Figure 2(b) shows the cross section of the sphere by the plane $(1\bar{1}0)$ that includes all principal axis of the cubic crystal ([111], [11$\bar{1}$], [001], and [110]). The reflections are observed along the [111], [11$\bar{1}$], and [001] directions and no intensity is visible along the

[110] direction. This observation is unusual from the point of view of the Back-Jensen theory.[5] The anisotropic energy that fixes the orientation of the helix wave vector is given by the expression[16]

$$E_{AN} = FL(\hat{k}) = 2F \sin^2 \vartheta(\sin^2 \varphi \cos^2 \varphi + \cos^2 \vartheta), \quad (5)$$

where $L(\hat{k})$ is a cubic invariant determining the **k** orientation relative to the crystal axes (ϑ and φ are the corresponding angles) and F is the strength of the anisotropic interactions determined by the cubic anisotropy and the anisotropic exchange. The cubic invariant describes the energy landscape with $L(\hat{k})$ minimal and is equal to 0 when $\hat{k} \| \langle 100 \rangle$ and $L(\hat{k})$ is maximal and is equal to 2/3 when $\hat{k} \| \langle 111 \rangle$. The $\langle 110 \rangle$ directions are saddle points. Therefore, the orientation of **k** is fixed along the $\langle 100 \rangle$ axes if constant $F > 0$ and along the $\langle 111 \rangle$ axes if constant $F < 0$. The simultaneous appearance of the orientation **k** along $\langle 100 \rangle$ and $\langle 111 \rangle$ axes means that the constant F is a value spatially fluctuating around zero. This ill-defined orientation of the wave vector **k** in given case is caused by a disorder induced by Fe doping into the pure MnSi compound. One can suppose that the doping induces randomness in the local anisotropy and, therefore, unpins partially the directions of spirals. The similar phenomenon is observed in FeGe ($T_c = 287$ K), when the anisotropy constant F changes sign at $T \sim 220$ K from positive (**k** along $\langle 100 \rangle$) at high temperatures to negative (**k** along $\langle 111 \rangle$) at low temperatures. The transition in the orientation undergoes with temperature hysteresis with the width of order of 20 K within which range two orientations of the **k** vector may coexist.[22]

C. Magnetic-field evolution

As is well known[1,2,15,16] the magnetic field affects strongly the helix structure of the pure MnSi system. The transformations under applied magnetic field are very typical for all compounds under study. The magnetization $M(H)$ and magnetic susceptibility $\chi(H) = dM/dH$ measured at $T = 2$ K and $T = 10$ K for the representative compound with $y = 0.08$ are shown in Figs. 3(a) and 3(b), respectively.

The magnetization increases linearly with the magnetic field changing the slope in the field range $H \approx H_{C1}$. This corresponds to the process of reorientation of the helix domains along the field axis shown in Fig. 4. In the scattering picture it is seen as an accumulation of the intensity of the different Bragg spots to the single one with **k** along the field. The threshold field H_{C1} can be defined as a field which suppresses the crystal anisotropy and forms the single domain of the conical spirals. With further increase in the magnetic field magnetization demonstrates the linear dependence up to the field H_{C2}, where it saturates indicating the field-induced phase transition from the conical to the ferromagnetic state. The Bragg spots vanish at $H = H_{C2}$. The peculiarities of the $M(H)$ dependence and different slopes χ_1 and χ_2 are well revealed in the $\chi(H)$ dependence.

The similar change in the slope in the magnetization curve at H_{C1} was observed in the relative compounds $Fe_{1-x}Co_xSi$ (see Ref. 18). It was interpreted as a consequence

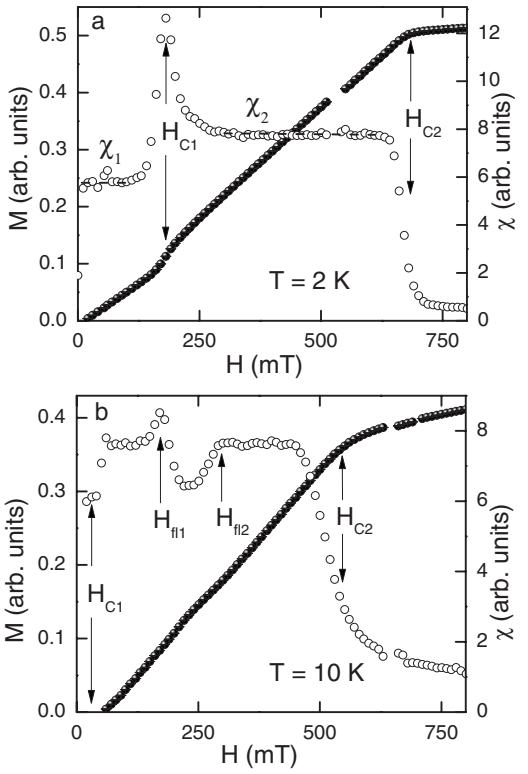

FIG. 3. Magnetic-field dependence of the magnetization M and susceptibility χ taken at $T = 2$ K (a) and $T = 10$ K (b) for $Mn_{0.92}Fe_{0.08}Si$ compound.

of the unusual form of the magnetic energy of the helical structure, which for the unit cell is given by[13]

$$E_{\mathrm{Mag}} = -g\mu_B S\left[\frac{H_\parallel^2}{2H_{C2}} + \frac{H_\perp^2 \Delta^2}{4H_{C2}[\Delta^2 - (g\mu_B H_\perp)^2/2]}\right] + FL(\hat{k}), \quad (6)$$

where S is the total spin of the unit cell, $H_\parallel$ and $H_\perp$ are the field components along and perpendicular to the helix wave vector **k**, and Δ is the spin-wave gap. The first term with $H_\parallel$ is a classical part of the Zeeman energy. The second one has a quantum origin and it describes the interaction of the field, perpendicular to **k**, with the helix as an individual entity. The third term is the cubic anisotropy and anisotropic exchange given by Eq. (5).

In a weak magnetic field $H < H_{C1}$, when the directions of the helix axes **k** are frozen by the local anisotropy, the **k** vectors have different orientations with respect to the magnetic field. The components of the magnetic field can be given as $\langle H_\parallel^2 \rangle = \eta H^2$ and $\langle H_\perp^2 \rangle = (1-\eta)H^2$, where η is the average value of the square of the cosine of the angle between the field and helix wave vector **k**. In this case the magnetic energy is $E_{\mathrm{Mag},1} = -g\mu_B SH^2(1+\eta)/(4H_{C2})$, where the L term is taken into account as a source of the anisotropy keeping **k** noncollinear to **H**. In a strong field $H > H_{C1}$, when the **k** vector is along the field direction and $H_\perp = 0$, then $E_{\mathrm{Mag},2} = -g\mu_B SH^2/(2H_{C2})$. The magnetic susceptibility is determined as

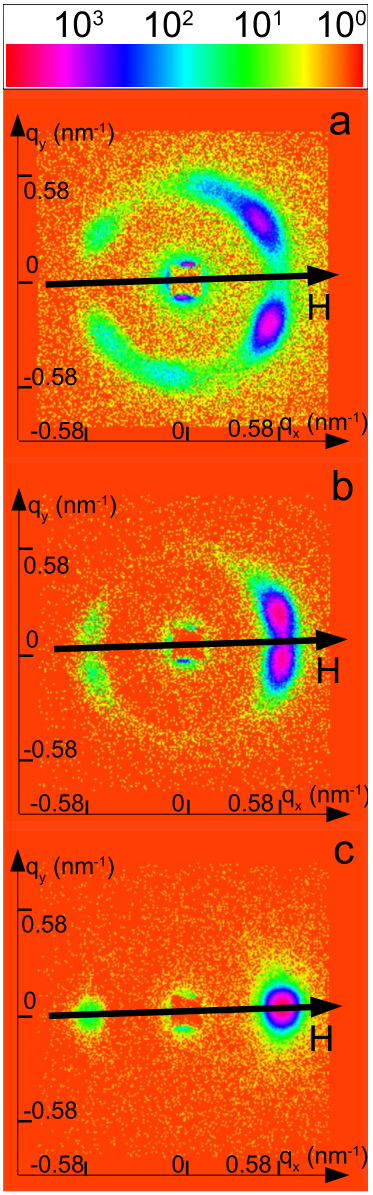

FIG. 4. (Color online) Maps of the polarized SANS intensities of the $Mn_{0.92}Fe_{0.08}Si$ compound under applied magnetic field $H=20$ mT (a), 50 mT (b), and 120 mT (c) at $T=8$ K.

$$\chi = -\frac{1}{H}\frac{dE_{\mathrm{Mag}}}{dH} \tag{7}$$

and one obtains for the ratio of two susceptibilities in the weak and strong magnetic fields

$$\frac{\chi_1}{\chi_2} = \frac{1+\eta}{2}. \tag{8}$$

In case of the randomly orientated helix axes $\eta=1/3$ and the ratio $\chi_1/\chi_2=2/3$. This theoretical prediction is in agreement with the experimental data presented in Fig. 3(a). Indeed, the ratio of the two slopes $\chi_1/\chi_2 \approx 0.70$. Thus the crossover observed in the magnetization curve is explained by the presence of the second field-dependent term (quantum term $\sim H_\perp$) in the expression of the magnetic energy [Eq. (6)].

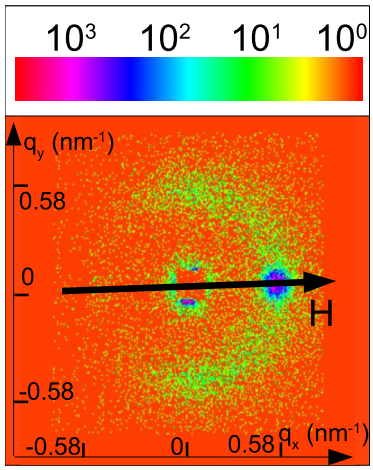

FIG. 5. (Color online) Map of the polarized SANS intensity of the $Mn_{0.92}Fe_{0.08}Si$ compound under applied magnetic field $H=200$ mT at $T=10$ K.

An interesting feature in the magnetic-field behavior takes place near T_c. There is a **k**-flop region, where helix instability occurs and spin helices undergo the 90° jump from $\mathbf{k}\|\mathbf{H}$ to $\mathbf{k}\perp\mathbf{H}$. In the neutron diffraction experiment it is seen as decrease in the intensity of the Bragg reflection at $\mathbf{q}=\mathbf{k}\|\mathbf{H}$, while a new Bragg spot appears at $\mathbf{k}\perp\mathbf{H}$. The typical SANS pattern for the **k**-flop phase is shown in Fig. 5. The integral intensity of the Bragg reflection (at $\mathbf{k}\|\mathbf{H}$) shows a deep minimum at $H_{\mathrm{fl}}=200$ mT seen in Fig. 6. The increase in the scattering intensity at $\mathbf{q}=\mathbf{k}\perp\mathbf{H}$ is shown in the inset of Fig. 6.

To interpret this **k**-flop phenomenon we consider again the evolution of the helical structure upon increasing magnetic field on the basis of Eq. (6). Close to T_c the term $GL(\hat{k})$ is very small and it can be neglected. Hence the direction of the helix vector **k** is determined by the competition of the first two terms in Eq. (6). The first one ($\sim H_\parallel^2$) tends to orient the helix wave vector **k** along the field, while the second one ($\sim H_\perp^2$) favors the orientation of **k** perpendicular to **H**. If

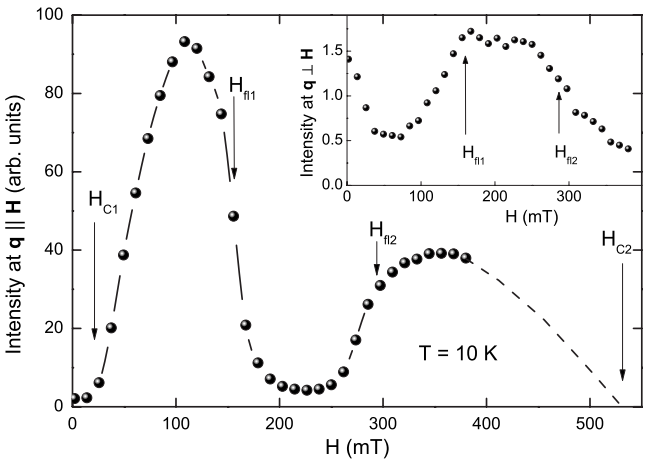

FIG. 6. The field dependence of the integral SANS intensity at $\mathbf{k}\|\mathbf{H}$ for the $Mn_{0.92}Fe_{0.08}Si$ compound at $T=10$ K. The inset gives the field dependence of the integral SANS intensity at $\mathbf{k}\perp\mathbf{H}$.

$g\mu_B H \ll \Delta$ the first term is dominant and **k** is parallel to the magnetic field. If the field approaches the value $\sqrt{2}\Delta/g\mu_B$, the orientation of $\mathbf{k} \perp \mathbf{H}$ becomes more favorable as both terms are negative. When $g\mu_B H > \sqrt{2}\Delta$ the second term is unreasonable[13] and **k** returns back to the field axis. Therefore, the field value associated with the top field boundary of the **k**-flop phase is denoted as H_{gap}.

This scenario is exactly observed in this paper as well as for $Fe_{1-x}Co_xSi$ in Ref. 18. So we observe the **k** flop under an applied field from one energetically favorable direction (parallel to the field) to the other (perpendicular to it). This **k** flop gives the experimental evidence for the spin-wave gap $\Delta \sim g\mu_B H_{\text{fl}}/\sqrt{2}$. (For $Mn_{0.92}Fe_{0.08}Si$, e.g., $\Delta \approx 28$ μeV.) As was shown in Ref. 13 the major contribution to the spin-wave gap in zero field stems from the interaction between spin waves and is determined by the DM interaction $\Delta_{\text{SW}}^2 = d[H_{C2}^2/(4S)]$, where the numerical coefficient $d \sim 1$ cannot be evaluated. Upon decrease in the temperature the anisotropy expressed by the last term in Eq. (6) arises and, thus, changes the energy landscape not allowing the easy **k** flop at $H \sim H_{\text{fl}}$ (see for example Ref. 16).

III. (*H-T*) PHASE DIAGRAMS AND PRINCIPAL INTERACTIONS

A. (*H-T*) phase diagram

The experimental findings of Sec. II are summarized in the *H-T* phase diagrams. The critical fields H_{C1} and H_{C2} are plotted as a function of temperature in Fig. 7 for the compounds with $y=0.06$, 0.08, and 0.10. Well below T_c these two fields determine the state of the magnetic system. In the range of the fields $0 < H < H_{C1}$ the spin helix structure occurs in the multidomain state with the **k** vector oriented along principal directions of the cube. For pure MnSi these directions are the four ⟨111⟩ axes. The increase in Fe concentration leads to some disorientation of **k** and to enhancement of additional Bragg peaks along ⟨100⟩. In the field range between H_{C1} and H_{C2} the samples are single domain with the conical spin structure along the field axis ($\mathbf{k} \| \mathbf{H}$). The fields above H_{C2} force the spin structure to be ferromagnetically ordered.

Note that the value of the critical temperature was determined as the point where the shape of the peak in q dependence changes from the Gaussian below T_c to the Lorentzian above T_c. Thus determined T_c coincides with the temperature where the Bragg peaks transform into the half-moon images of the critical scattering coming from the fluctuations [see Fig. 1(b)]. They are equal to $T_c = 28.8 \pm 0.05$, 16.5 ± 0.05, 10.55 ± 0.05, and 6.8 ± 0.05 K for the samples with $y=0.0$, 0.06, 0.08, and 0.10, respectively.

These compounds show unusual behavior in the critical temperature range. Just below T_c a flop of the helix wave vector **k** occurs in a certain field range. It is seen as a 90° jump of the wave vector from $\mathbf{k} \| \mathbf{H}$ to $\mathbf{k} \perp \mathbf{H}$. The field H_{fl} in Fig. 7 (triangles) shows the boundary of the **k**-flop phase. The upper field boundary of the **k**-flop phase is prescribed to the field H_{gap} corresponding to the spin-wave gap (see interpretation above). Just above T_c for all compounds $Mn_{1-y}Fe_ySi$ the magnetic structure melt into the fluctuations

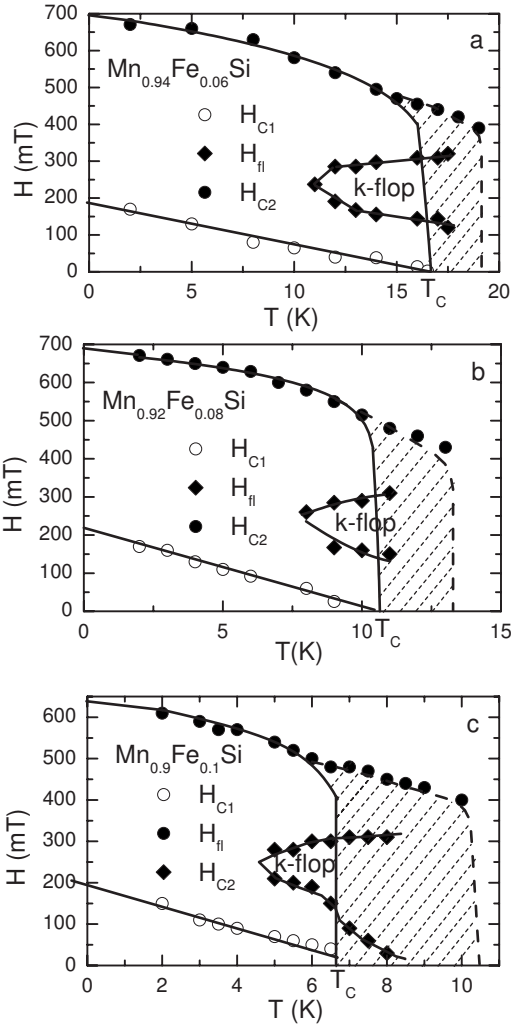

FIG. 7. (*H-T*) phase diagrams for $Mn_{0.94}Fe_{0.06}Si$ (a), $Mn_{0.92}Fe_{0.08}Si$ (b), and $Mn_{0.9}Fe_{0.1}Si$ (c) compounds.

of helix structure with random orientations the wave vector **k**. The half moons of intensity are well visible in this temperature range $T_c < T < T^*$ and under magnetic field $H < H_{C2}$. We marked this range by the dashed lines in the $H-T$ phase diagrams. The **k**-flop phase overlaps partially with this dashed critical range since the **k** flop is visible above the critical temperature as well. It is found that the interval $\Delta T^* = T^* - T_c$ widens with doping y: $\Delta T^* \approx 0.9$ K, 2 K, 2.4 K, and 3.5 K for $y=0$, 0.06, 0.08, and 0.10, respectively.

B. Hierarchy of principal interactions

The (*H-T*) phase diagrams shown in Fig. 7 are typical for the cubic helical magnets including the ternary compounds under study $Mn_{1-y}Fe_ySi$ and the compounds $Fe_{1-x}Co_xSi$ studied in Refs. 17 and 18. The similarity of the (*H-T*) phase diagrams suggests that their magnetic systems are governed by the same set of the interactions whose interplay determines the values of the critical fields H_{C1}, H_{C2}, and $H_{\text{gap}} = H_{\text{fl2}}$ as well as the value of the helix wave vector **k**. The concentration dependences of these four parameters are shown in Fig. 8. Here H_{C1} and H_{C2} are determined as values

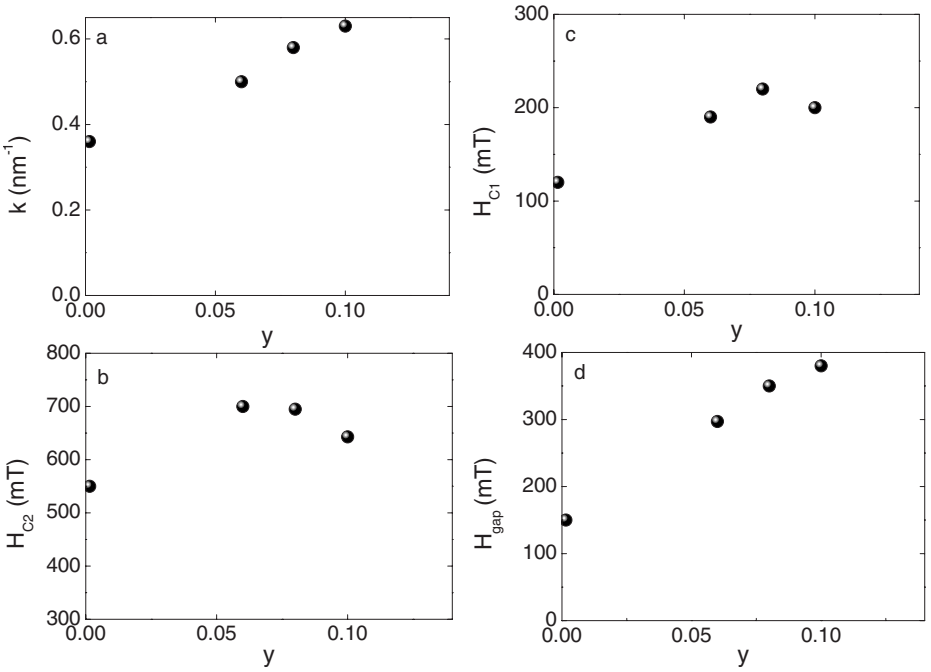

FIG. 8. Dependence of the helix wave vector k (a), the critical field H_{C2} (b), the critical field H_{C1} (c), and the field H_{gap} (d) on the Fe concentration y for $Mn_{1-y}Fe_ySi$ compounds.

taken at the lowest measured temperature. The value of the helix wave vector $|\mathbf{k}|=k=2\pi/d$ changes significantly [Fig. 8(a)] showing a linear increase from 0.35 to 0.63 nm^{-1} with doping y, i.e., the helix length shortens from 185 to 100 Å. The values of H_{C1} [Fig. 8(c)] and H_{fl2} [Fig. 8(d)] increases with doping as well. The value of H_{C2} [Fig. 8(b)] demonstrates relatively small changes.

As is explained in Sec. I, the phase diagram and the values of H_{C1}, H_{C2}, k, and H_{gap} are well interpreted within the theory recently developed by one of the authors (see Ref. 13) on the basis of the Bak-Jensen model.[5] The theory suggests that using Eqs. (1)–(4) one is able to estimate the major driving interactions of the magnetic system, such as the anisotropy constant $F\sim 2g\mu_B H_{C1}/k^2$, the spin-wave stiffness $A=g\mu_B H_{C2}/k^2$, the Dzyaloshinskii constant $SD=Ak$, and the spin-wave gap $\Delta\sim g\mu_B H_{gap}/\sqrt{2}$. The calculated energies of the principal interactions F/a^2, A/a^2, SD/a, and Δ are shown in Fig. 9 as a function of y (here a is the lattice parameter).

The exchange energy A/a^2 decreases linearly from 2.4 to 0.8 meV [Fig. 9(a)]. The extrapolation (dashed line) gives the critical concentration $y\approx 0.15$ where the spin-wave stiffness (and, consequently, the exchange interaction) becomes zero. Apparently it is a result of frustrations enhancing with the Fe doping. The energy of DM interaction coupled to the average spin SD has a moderated decrease from 0.4 to 0.25 meV. [Fig. 9(b)]. The anisotropy constant F/a^2 decreases with doping y [Fig. 9(c)] that correlates to the disorientation

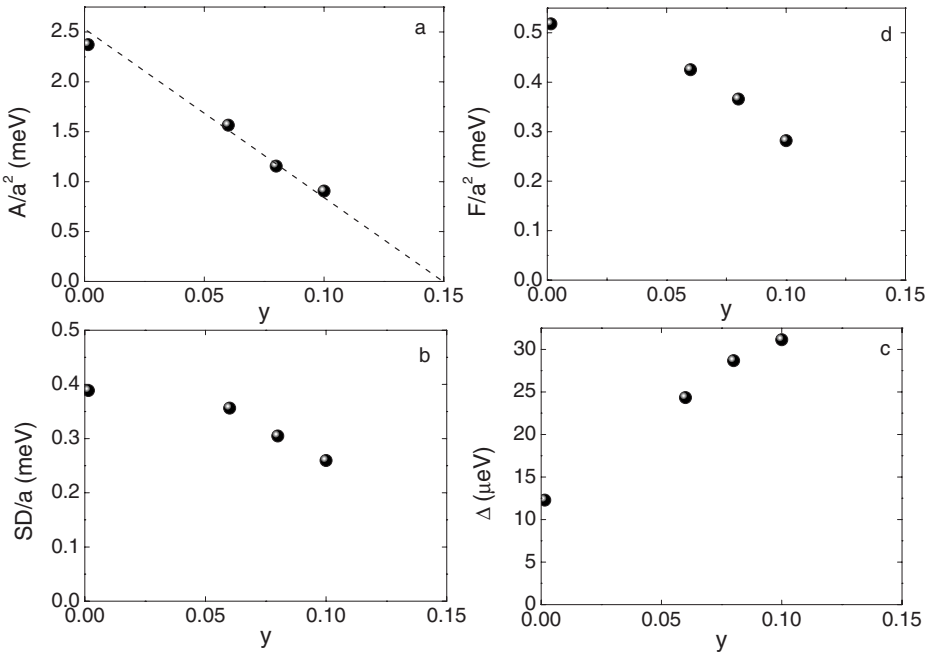

FIG. 9. Dependence of the estimated values of the exchange energy of the order A/a^2 (a), DM energy SD/a (b), the anisotropy constant F/a^2 (c) and the spin-wave gap Δ (d) on the Fe concentration y for $Mn_{1-y}Fe_ySi$ compounds.

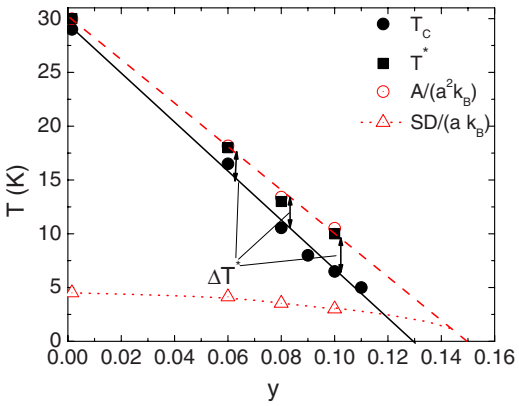

FIG. 10. (Color online) Critical temperatures (T_c and T^*), and spin-wave stiffness $A/(a^2k_B)$ along with the Dzyaloshinskii constant $SD/(ak_B)$ as functions of the Fe concentration y.

of the **k** vector in the doped systems. Opposite to these three, the spin-wave gap Δ linearly increases from value 12 to 30 μeV [Fig. 9(d)].

Remarkable though that this set of the principal interactions is able to explain the concentration dependence of the critical temperature T_c plotted in Fig. 10. T_c is well seen to decrease linearly with the Fe concentration y in agreement with the early studies (see Ref. 11 and references therein). This tendency and its extrapolation suggest that the Fe doping can lead this system to the quantum phase transition at $y \approx 0.13$. Indeed, the increase of the non-thermal parameter, the concentration y, results in T_c approaching 0, which is, by definition, the Quantum Critical Point (QCP). This concept enables us to model the behavior of the system close to the QPT using the Fe concentration as a nonthermal parameter. Now we can follow the evolution of the system on the way to the QPT using the estimations of the principal interactions and how they change with doping y.

To compare the spin-wave stiffness with T_c, we plot the value of $A/(a^2k_B)$ on the same graph as T_c in Fig. 10. It should be noted that both values have the same linear behavior as a function of y and the two lines displace close to one another in the (T-y) phase diagram. Nevertheless, the calculated points of $A/(a^2k_B)$ lay somewhat higher than the experimental T_c ones leaving a space for a new partially ordered magnetic state. Indeed, the values of T^*, the upper boundary of the partially disordered phase, coincides practically with the values of $A/(a^2k_B)$. For completeness, we added the y dependence of $SD/(ak_B)$ to Fig. 10.

IV. DISCUSSION

As is well known the hierarchy of interactions determines the magnetic properties of the $Mn_{1-x}Fe_xSi$ compounds. The competition of two interactions is stabilized in the helix spin structure with the wave vector **k**, which length is, by definition, the ratio SD/A. As k increases with concentration y [Fig. 8(a)], then one can expect that influence of DM interaction increases compared to the isotropic exchange interaction. The comparison of energies (A and SD) plotted in the (T-y) phase diagram (Fig. 10) shows that value of SD/ak_B

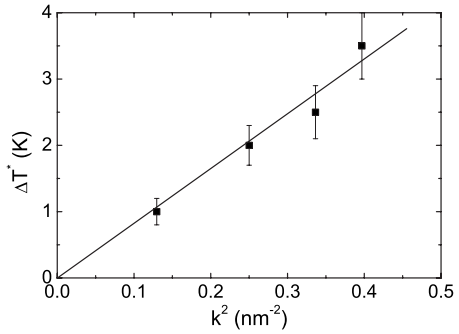

FIG. 11. Dependence of the temperature ΔT^* on the squared the wave vector. The line is the fit $\Delta T^* = C(ka)^2$ with $C = 3.5 \pm 0.3$ K.

becomes of the same order as A/a^2K_B in the region $0.13 \leq y \leq 0.15$. The ordering temperature T_c is clearly determined by the decreasing value of the isotropic exchange interaction. On the other hand, the existence of the fluctuating disordered phase below T^* and above T_c is related to the DM interaction. We relate the temperature range, where the ring of scattering is visible $\Delta T^* = T^* - T_c$ with the value of the wave vector k. The dependence of ΔT^* versus square of the wave vector k^2 for the all samples is shown in the Fig. 11. The experimental points ΔT^* linearly depends on k^2 [$\Delta T^* = C(ka)^2$ with $C = 3.5 \pm 0.3$ K], giving the experimental proof for existence of the critical temperature range with the dominating influence of the DM interaction. It is interesting to note that the critical fluctuations above T_c were studied in the mean-field approximation in.[23] It was shown there that DM interaction renormalizes the transition temperature and we have $T_c = T_{c0} + C'k^2$. It can be that observed above the partially ordered state is a result of this renormalization. However, analysis of this problem is out of the scope of this paper.

Finally, the phase diagram (Fig. 7) shows the paramagnetic state above T^*, orientationally disordered fluctuating state in the narrow range between T^* and T_c and the ordered helix state below T_c. The linear approximation $T_c \to 0$ gives the critical concentration $y_c = 0.13$ at which the ordered state could not be observed. The compound with $y_c = 0.13$ should have rather complicated picture of the critical phenomena, which can possibly mimic the conditions of the quantum phase transition.

The (T-y) phase diagram of the $Mn_{1-y}Fe_ySi$ compounds (Fig. 10) and the (T-P) phase diagram of pure MnSi (Fig. 6 in Ref. 24) duplicate one another. In the former and latter cases the increase in y and P, respectively, results in the decrease in T_c. From the parameters k and H_{C2} of these compounds we have estimated the values of the principal interactions A and SD. It should be noted that neither k nor H_{C2} change with the increase in the pressure in MnSi. Thus one concludes that principal interactions (A and SD) do not change under applied pressure, implying another "hidden" parameter that causes changes in T_c under the pressure. Comparison of two phase diagrams, which look so similar, however, shows that they are driven by the different interactions. In case of the (T-y) phase diagram of the $Mn_{1-y}Fe_ySi$ compounds the critical temperature is clearly determined by the exchange integral. The exchange integral decreases with

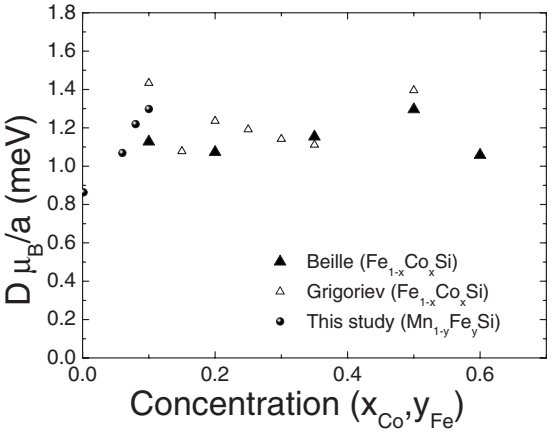

FIG. 12. Dependence of the DM constant D/a on the Fe concentration y for $Mn_{1-y}Fe_ySi$ compounds and Co concentration x for $Fe_{1-x}Co_xSi$ compounds.

Fe doping due to competition between ferromagnetic (Mn-Mn) and antiferromagnetic (Mn-Fe) bonds as it is often observed in the binary alloys of the 3*d* metals. In case of the (*T*-*P*) phase diagram of pure MnSi the hidden parameter drives the system to the disordered state. As has been noticed in Sec. I the hidden parameter was suggested to be the spin-wave gap Δ^2, which consists of two parts: the positive one, determined by DM interaction, and the negative one, determined by the magnetoelastic interaction.[14] Presumably, the quantum phase transition occurs when $\Delta^2=0$.

In our estimations using Eqs. (1)–(4) the value of the DM interaction is coupled to the average spin per unit cell SD/a. In fact the average spin changes with the concentration y and, therefore, it is interesting to obtain the true numbers for the Dzyaloshinskii constant $\mu_B D/a$. The values of the average spin can be found in Ref. 11 and after division to the value of $\langle S\rangle$ one obtains the numbers of $\mu_B D/a$ for different concentrations of y. For completeness, we calculated thus obtained values of $\mu_B D/a$ for the other compound $Fe_{1-x}Co_xSi$ described in Refs. 17 and 18. The combined data are shown in Fig. 12. The obtained numbers for the Dzyaloshinskii constant $\mu_B D/a$ fluctuate around value of 1.15 ± 0.1 meV. Thus, one can conclude that the Dzyaloshinskii constant D/a does not depend on the concentration of these compounds (either $Mn_{1-y}Fe_ySi$ or x for $Fe_{1-x}Co_xSi$) and is the intrinsic number inherent to the crystallographic structure with the symmetry $P2_13$ and the lattice constant of order of 0.45 nm.

V. CONCLUDING REMARKS

We have carried out polarized neutron diffraction experiments to study the magnetic structure in $Mn_{1-y}Fe_ySi$ single crystals with $y=0$, 0.06, 0.08, and 0.10. Below T_c in zero field $Mn_{1-y}Fe_ySi$ is shown to have a multidomain helix structure. Increasing of the Fe concentration y results in rise of the disorder inside the compound: if for small y the helix axis orients along the $\langle 111\rangle$ direction, then for $y\geq0.06$ the helix wave vector **k** has a tendency to reorientation of the wave vector to $\langle 100\rangle$. The magnetic field induces a single domain structure with the helix wave vector oriented along the field axis at $H=H_{C1}$. The field H_{C1} determines the energy of the magnetic anisotropy. In the vicinity of T_c the field-dependent integral intensity of the Bragg reflection shows a sharp minimum at $H=H_{\rm gap}$. This phenomenon is well explained by the presence of a spin-wave gap $g\mu_B H_{\rm gap}/\sqrt{2}$ that provides the stability of the spin-wave spectrum with respect to the perpendicular magnetic field. Further increase in the applied field leads to a magnetic phase transition from a conical to a ferromagnetic state close to H_{C2}. On the basis of these measurements we have built the (*H*-*T*) phase diagrams for each compound.

These phase diagrams show that the same set of parameters governs the magnetic system in these compounds. Furthermore, we have evaluated the major interactions of the system *A*, *D*, *F*, and Δ from our the experiment using the theory.[13] As was found the spin-wave stiffness constant A/a^2 resembles the behavior of the critical temperature T_c decreasing linearly with y but the spin-wave gap Δ, on the contrary, increases with y. Thus, we demonstrate that the isotropic exchange interaction determines T_c in these compounds.

The DM interaction influences significantly the critical phenomena in these compounds. We demonstrate the enhancement of the fluctuating helical phase in the narrow temperature range $T_c<T<T^*$. The temperature range ΔT^*, where this phase occurs, is found to be proportional to k^2. This range increases with increase in y and, though is noticeable for pure MnSi, is especially important at $y\geq0.1$. Further detailed study of the compound with $y_c\sim0.13$ is very desirable to realize the peculiar situation when the isotropic exchange *A* is zero but the DM interaction has a finite value.

ACKNOWLEDGMENTS

The PNPI team acknowledges GKSS for their hospitality. The work was supported in part by the RFBR Project No. 07-02-01318 and the Russian State Programs "Quantum Macrophysics" and "Strongly correlated electrons in semiconductors, metals, superconductors, and magnetic materials" and Russian State Program "Neutron research of solids."

[1] Y. Ishikawa, K. Tajima, D. Bloch, and M. Roth, Solid State Commun. **19**, 525 (1976).
[2] Y. Ishikawa, G. Shirane, J. A. Tarvin, and M. Kohgi, Phys. Rev. B **16**, 4956 (1977).
[3] G. Shirane, R. Cowley, C. Majkrzak, J. B. Sokoloff, B. Pagonis, C. H. Perry, and Y. Ishikawa, Phys. Rev. B **28**, 6251 (1983).
[4] I. E. Dzyaloshinskii, Zh. Eksp. Teor. Fiz. **46**, 1420 (1964) [Sov. Phys. JETP **19**, 960 (1964)]
[5] P. Bak and M. H. Jensen, J. Phys. C **13**, L881 (1980).
[6] O. Nakanishi, A. Yanase, A. Hasegawa, and M. Kataoka, Solid

State Commun. **35**, 995 (1980).
[7] M. Kataoka and O. Nakanishi, J. Phys. Soc. Jpn. **50**, 3888 (1981).
[8] C. Pfleiderer, G. J. McMullan, S. R. Julian, and G. G. Lonzarich, Phys. Rev. B **55**, 8330 (1997).
[9] C. Pfleiderer, S. R. Julian, and G. G. Lonzarich, Nature (London) **414**, 427 (2001).
[10] C. Pfleiderer, D. Resnik, L. Pintschovius, H. Von Lohneysen, M. Garst, and A. Rosch, Nature (London) **427**, 227 (2004).
[11] N. Manyala, Y. Sidis, J. F. DiTusa, G. Aeppli, D. P. Young, and Z. Fisk, Nature (London) **404**, 581 (2000).
[12] N. Manyala, Y. Sidis, J. F. DiTusa, G. Aeppli, D. P. Young, and Z. Fisk, Nature Mater. **3**, 255 (2004).
[13] S. V. Maleyev, Phys. Rev. B **73**, 174402 (2006).
[14] S. V. Maleyev, J. Phys.: Condens. Matter **21**, 146001 (2009).
[15] S. V. Grigoriev, S. V. Maleyev, A. I. Okorokov, Yu. O. Chetverikov, and H. Eckerlebe, Phys. Rev. B **73**, 224440 (2006).
[16] S. V. Grigoriev, S. V. Maleyev, A. I. Okorokov, Yu. O. Chetverikov, P. Böni, R. Georgii, D. Lamago, H. Eckerlebe, and K. Pranzas, Phys. Rev. B **74**, 214414 (2006).
[17] S. V. Grigoriev, V. A. Dyadkin, D. Menzel, J. Schoenes, Yu. O. Chetverikov, A. I. Okorokov, H. Eckerlebe, and S. V. Maleyev, Phys. Rev. B **76**, 224424 (2007).
[18] S. V. Grigoriev, S. V. Maleyev, V. A. Dyadkin, D. Menzel, J. Schoenes, and H. Eckerlebe, Phys. Rev. B **76**, 092407 (2007).
[19] Y. Nishihara, S. Waki, and S. Ogawa, Phys. Rev. B **30**, 32 (1984).
[20] S. V. Grigoriev, D. Chernyshov, V. A. Dyadkin, V. Dmitriev, S. V. Maleyev, E. V. Moskvin, D. Menzel, J. Schoenes, and H. Eckerlebe, Phys. Rev. Lett. **102**, 037204 (2009).
[21] The schematic outline of the experiment can be found in Ref. 16 (Fig. 3).
[22] B. Lebech, J. Bernhard, and T. Freltoft, J. Phys.: Condens. Matter **1**, 6105 (1989).
[23] S. V. Grigoriev, S. V. Maleyev, A. I. Okorokov, Yu. O. Chetverikov, R. Georgii, P. Böni, D. Lamago, H. Eckerlebe, and K. Pranzas, Phys. Rev. B **72**, 134420 (2005).
[24] C. Thessieu, C. Pfleiderer, A. N. Stepanov, and J. Flouquet, J. Phys.: Condens. Matter **9**, 6677 (1997).